Electronic Supplementary Material (ESI) for Lab on a Chip.
This journal is © The Royal Society of Chemistry 2022

Electronic Supplementary Information (ESI)

Mainstreaming microfluidic microbial fuel cells: a biocompatible membrane grown *in situ* improves performance and versatility

Lingling Gong,[a] Mehran Abbaszadeh Amirdehi,[a] Jayesh M. Sonawane,[a] Nan Jia,[a] Leon Torres de Oliveira,[a] Jesse Greener[a,*]

Département de chimie, Faculté des sciences et de génie,
Université Laval, Québec G1V 0A6, Canada; CHU de Québec,

Centre de recherche, Université Laval, Québec G1L 3L5, Canada;
Corresponding author - jesse.greener@chm.ulaval.ca

Table of contents:

1. Equivalent circuit used for EIS modeling

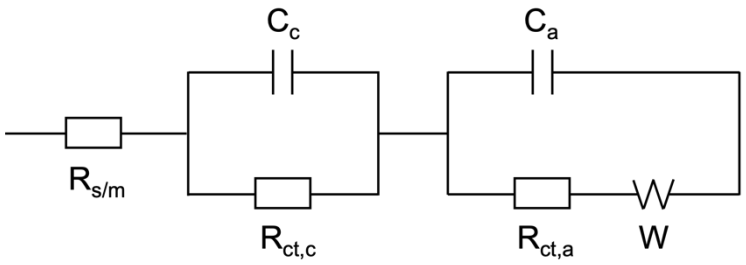

Fig. S1 The electrical equivalent circuit used to analyze the EIS data, including solution resistance ($R_{s/m}$), charge transfer resistances ($R_{ct,a}$ and $R_{ct,c}$), capacitances (C_a and C_c), and Warburg element (W).

2. EIS measurements under three flow conditions

Fig. S2 shows 3 Nyquist plots for a membraneless device under different flow rates. They were (i) balanced (Q_a=Q_c), (ii) imbalanced with over supply of acetate (Q_a>Q_c), (iii) and imbalanced with over supply of acetate (Q_c>Q_c). The differences in the ionic strength resulted in a chance in the solution resistance if the interface between the two streams changed position, thereby changing the percentage of the channel filled with anolyte and catholyte. In the case of the membraneless MFC, a change in the flow rate ratio resulted in the expected change in the solution resistance as marked in Fig. S2.

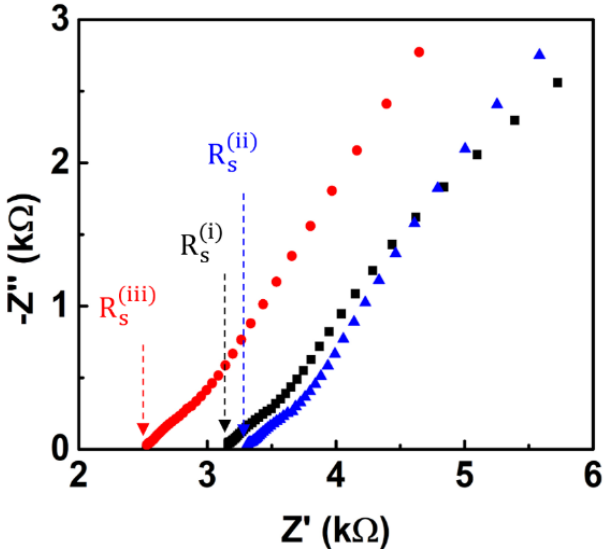

Fig. S2 Nyquist plot of a sterile 6 mm electrode gap membraneless MFC with a co-flow of anolyte (acetate solution, 10 mM) and catholyte (ferricyanide solution, 30 mM). Data reported for (i) Q_a=Q_c=0.5 mL h^{-1} (black), (ii) Q_a=0.7 mL h^{-1}, Q_c=0.3 mL h^{-1} (blue), and (iii) Q_a=0.3 mL h^{-1}, Q_c=0.7 mL h^{-1} (red).

However, for the membrane MFC, with a 50 µm membrane installed, no statistically significant changes to $R_{s/m}$ (the solution plus membrane resistance) were observed under the same flow rate ratios used for Fig. S2. Figure S3b shows a bar graph to better visualize the measured $R_{s/m}$ values and their statistical significance relative their standard deviations (via error bars).

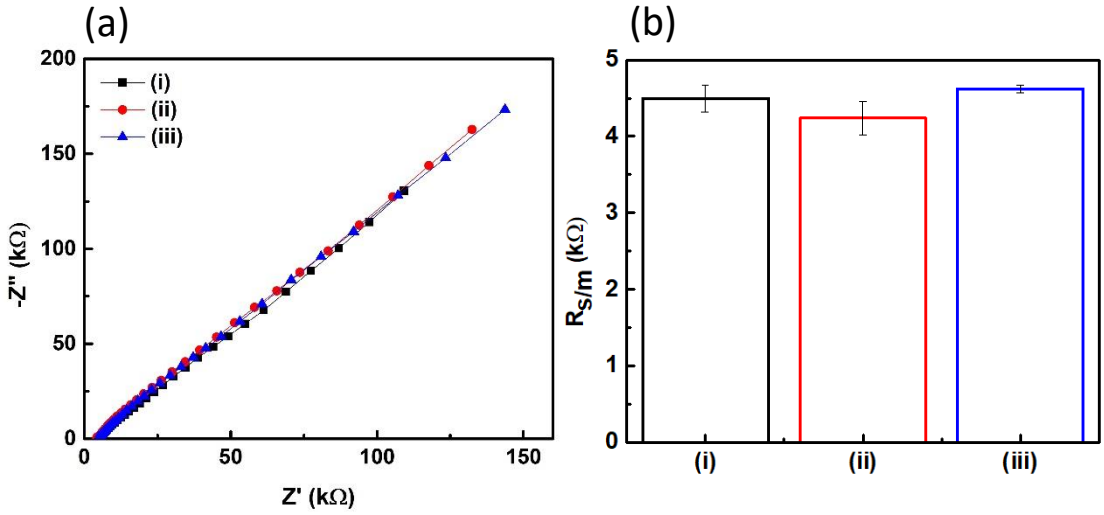

Fig. S3 Nyquist plot of a sterile 0.8 mm electrode gap membrane MFC with a co-flow of anolyte (acetate solution, 10 mM) and catholyte (ferricyanide solution, 30 mM). Colour coding matches that of Fig. S2.

3. Concentration contour lines in different locations

Next, we use simulations to visualize the differences in concentration at the top (PDMS/electrode) and bottom (glass) walls in a membrane device which is subjected to imbalanced flow conditions (assuming a constant 5 µm gap across the entire membrane length). This is a relevant question because the membrane gap is positioned at the glass wall. Thus, it is expected that the crossover will be more severe at the glass wall compared to the PDMS/electrode wall, which was a design feature to protect the electrodes from solution contamination. Fig. S4 contains contour lines for 2 mM acetate and 6 mM ferricyanide at top and bottom surfaces of the channel with under an imbalanced flow (Q_a=0.7 mL h^{-1} and Q_c=0.3 mL h^{-1}). The results show that the crossover is more pronounced at the glass side where the membrane gap is found, than at the PDMS/electrode side. Thus, the device can accommodate pressure imbalances without breaking, while limiting contamination of the electrodes. This is

especially important in MFCs where living biofilms on the anode can be irreversibly damaged by exposure to ferricyanide or oxygen in the catholyte.

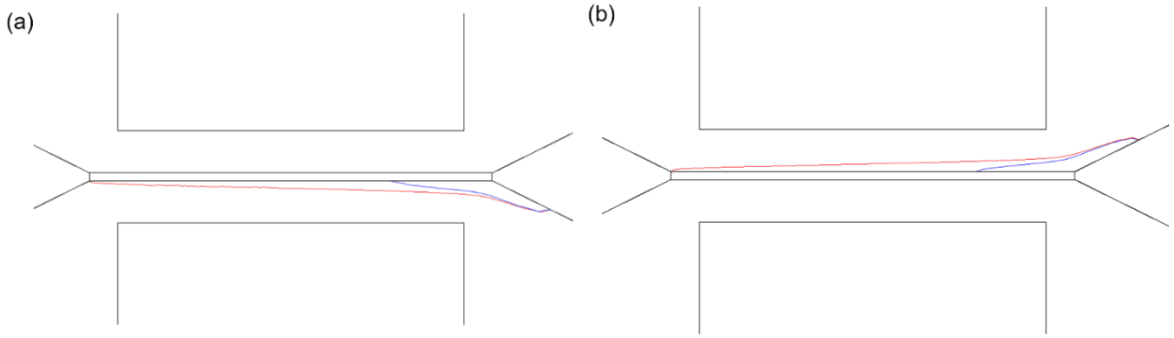

Fig. S4 Simulated results of the 2 mM acetate (a) and 6 mM ferricyanide (b) contours at the glass wall (red) and the PDMS/electrode wall (blue) for a membrane MFC (with 0.8 mm electrode distance) with membrane of 50 µm and a 5 mm gap at the glass surface. Flow rates of a 0 mM acetate (Q_a) and a 30 mM ferricyanide (Q_c) solutions were imbalanced, wich Q_a=0.7 mL h^{-1} and Q_c=0.3 mL h^{-1}.

6. Calculations of solution buffer capacity and pH

The pH of acetate nutrients after protons produced was calculated. The ions in acetate nutrients that can react with H^+ are $H_2PO_4^-$ (3.1 mM), HPO_4^{2-} (1.3 mM), CO_3^{2-} (4.7 mM), HCO_3^- (21.4 mM), and CH_3COO^- (10 mM). As the concentration of HCO_3^- is much higher than other ions, thus, HCO_3^- was used it to estimate the final pH of the nutrient solution after protons produced following acetate oxidation. The dissociation equation of carbon acid can be expressed (pK_a=6.35 at 25°C)[1]:

$$H_2CO_3 \leftrightharpoons HCO_3^- + H^+ \qquad \text{(Eqn. S1)}$$

According to the Henderson-Hasselbalch equation, the pH of the solution can be calculated:[2]

$$pH = pK_a + \log_{10}\frac{[HCO_3^-]}{[H_2CO_3]} \qquad \text{(Eqn. S2)}$$

With known initial pH of 6.8 and [Ac^-] of 10 mM, the initial H_2CO_3 concentration is calculated to be 7.6 mM. The produced protons (strong acid) reacts with HCO_3^- irreversibly, which consume HCO_3^- and produce H_2CO_3.

$$HCO_3^- + H^+ \rightarrow H_2CO_3 \qquad \text{(Eqn. S3)}$$

With maximum proton concentration of 6.8 mM produced at membrane, thus the $[HCO_3^-]$ = 21.4 mM-6.8 mM = 14.6 mM. The final $[H_2CO_3]$ = 7.6 mM + 6.8 mM = 14.4 mM. Therefore, the pH of nutrient following acetate oxidation can be estimated: $pH = pK_a + \log_{10}\frac{[HCO_3^-]}{[H_2CO_3]} = 6.35 + \log_{10}\frac{14.6}{14.4} = 6.4$. This is higher than the critical pH required for membrane dissolution (5.0), therefore, it is unlikely that the slight solution acidification will result in loss of membrane integrity.

Next, we calculated the acetate nutrient buffer capacity. The buffer capacity, β (mM pH^{-1}), can be calculated by the equation below:

$$\beta = 2.303C\frac{K_a[H^+]}{(K_a+[H^+])^2} \quad \text{(Eqn. S4)}$$

where C is the total buffer concentration, $[H^+]=10^{-pH}$, $K_a=10^{-pKa}$. Thus $C=[HCO_3^-] + [H_2CO_3]$ =21.4 mM + 7.6 mM = 29 mM. $\beta = 2.303 \times 29\ \text{mM} \times \frac{10^{-6.35}\times 10^{-6.8}}{(10^{-6.35}+10^{-6.8})^2} = 12.9$ mM (the concentration to change the pH by one unit around the pKa (approximately 7).

4. Simulation of solution crossover

In this section, we simulate the solution crossover for both the membrane and membraneless MFC devices (see Fig. S5a and S5b) under different flow ratios and different electrode separation distances. The simulation consisted of a flow rate ratio between a 10 mM acetate solution (with anolyte flow rate Q_a) co-flowing beside a 30 mM ferricyanide solution (with catholyte flow rate Q_c) with a total flow rate of $Q_T=Q_a+Q_c$=1 mL/h. An flow ratio imbalance factor was defined $I=(Q_a-Q_c)/Q_T\times 100\%$ and was modified by increasing the individual anolyte (acetate) and catholyte (ferricyand flow rate by while maintaining the total flow rate the same (Q_T=1 mL h^{-1}). We quantified the crossover by measuring the acetate concentration and percentage at the edge of the cathode closest to the anode as the simulation was changed by applying I in steps of 10% between I=0 to I=50%. For each value of I, the acetate concentration on the cathode edge was observed to decrease with increasing electrode separation distances. The process was repeated with a flow imbalance factor resulting from an oversupply of catholyte, yielding similar results (results not shown).

The first simulations were run on the membraneless MFC and results are shown in Fig. S5. In this case, we observed that it was impossible to achieve an acetate crossover concentration at the cathode edge that was less than 10% of the original concentration with I=50% even with 6 mm electrode separation distance. We conclude that even temporary flow imbalances, for example that cause the anode to be exposed to moderately elevated levels of (toxic) catholyte, could lead to irreparable harm to the living bacteria, and could be the source of underperformance of membranless MFCs in the literature.

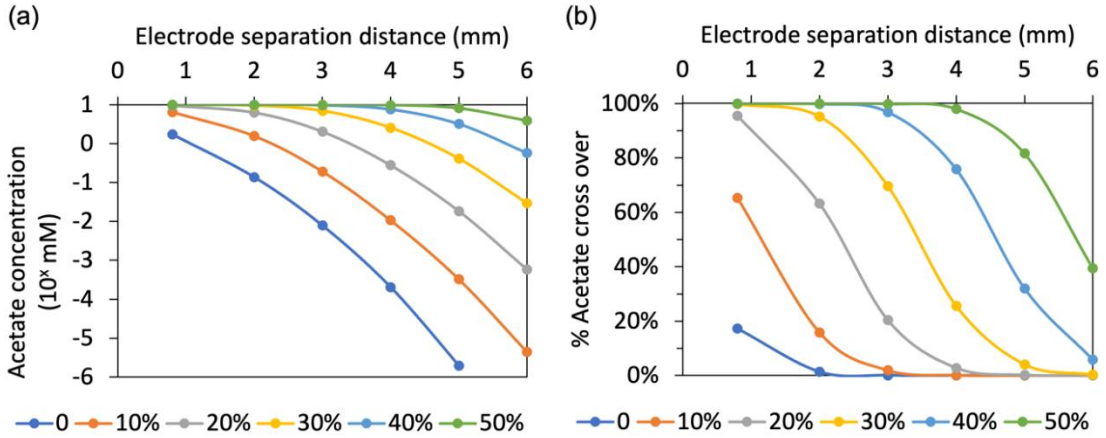

Fig. S5 Electrode separation distance study for a membraneless MFC. Plots showing the acetate concentration at the cathode edge as on a log scale (a) and on a linear scale (b) as acetate crossover concentration percentage as electrode separation is varied from 0.8 to 6 mm (b).

Next, the simulations were repeated on the membrane MFC device containing no membrane (acetate concentrations at the cathode edge on a log scale in Fig. S6a and on a linear scale in Fig. S6c) and with a membrane (acetate concentrations at the cathode edge on a log scale in Fig. S6b and on a linear scale in Fig. S6d). As expected without a membrane, the crossover was significant as electrodes were moved closer together and as the flow imbalance (I) was increased. However, with the chitosan membrane installed, the crossover was significantly reduced. For example, at an electrode separation of 0.8 mm only 0.13 mM acetate (1.3%) was observed at the cathode edge even with a flow imbalance ratio as high as I=50%. With an increased electrode separation distance, the simulated acetate concentration at the cathode edge became extremely small (below $1x10^{-6}$), therefore values at other separation distances are not shown in the Fig. S6b and S6d. We conclude that the membrane is very efficient in isolating the anolyte and catholyte chambers, even under strong flow imbalances and close electrode spacing.

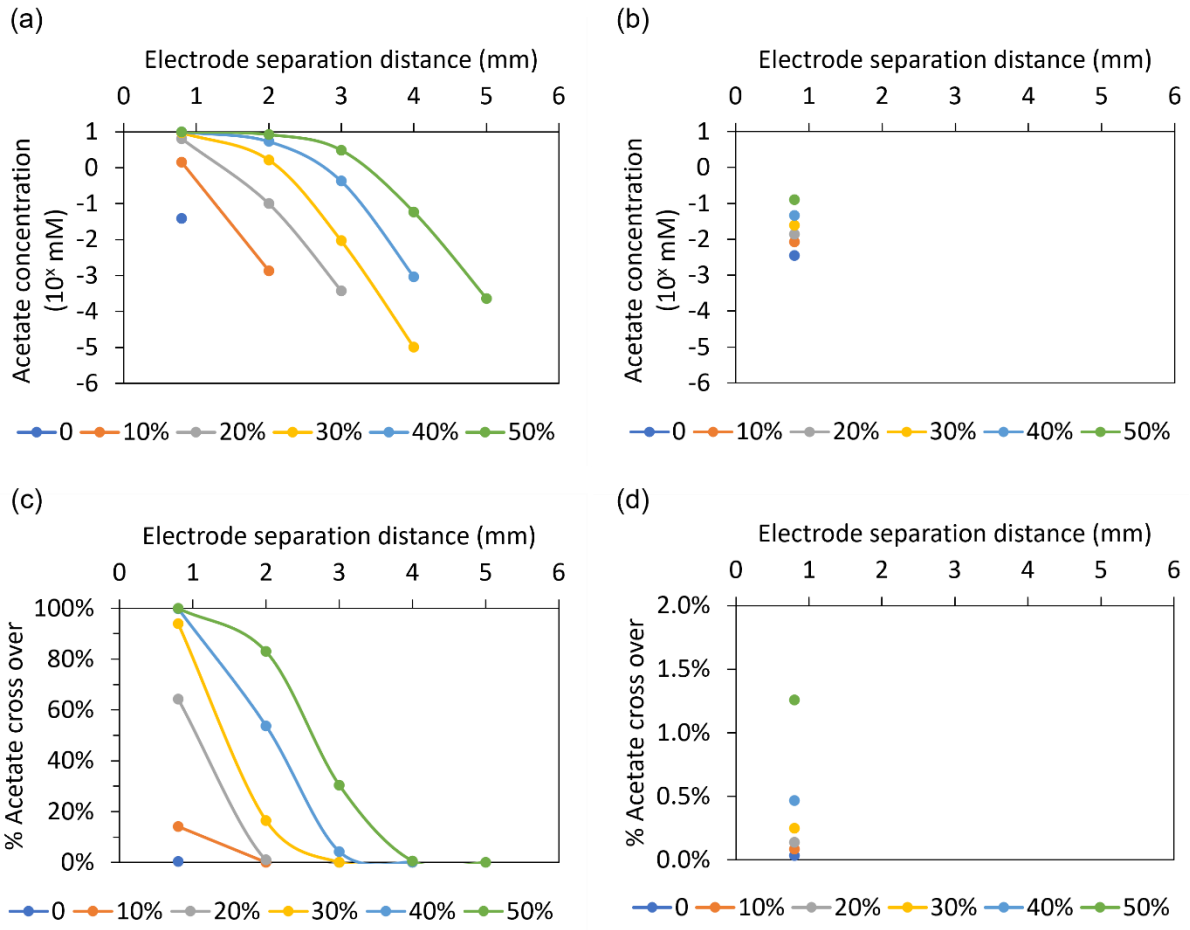

Fig. S6 Plot showing the acetate concentration at the cathode edge for a membrane device without (a, c) and with (b,d) the membrane installed. Crossover is measured in the vertical axis (a) and (b) in a log scale and (c), (d) in a linear scale as a percentage of the initial concentration. Initial concentrations were 10 mM for acetate and 30 mM for ferricyanide. The extremely small crossover concentrations for membrane-installed devices at separation distances of greater than 0.8 mm are not shown. Total flow rate was maintained at 1 mL h^{-1}. Colours represent different flow ratio imbalances, as defined in the main text.

6. Polarization test results

Polarization tests were used to obtain polarization curves (V vs. $\bar{I}_A$) and power density curves (area normalized power density ($\overline{P}_V$) vs. area normalized current ($\bar{I}_A$)). The process used was to switch between OCV and different R_{ext} values (Fig. S7).

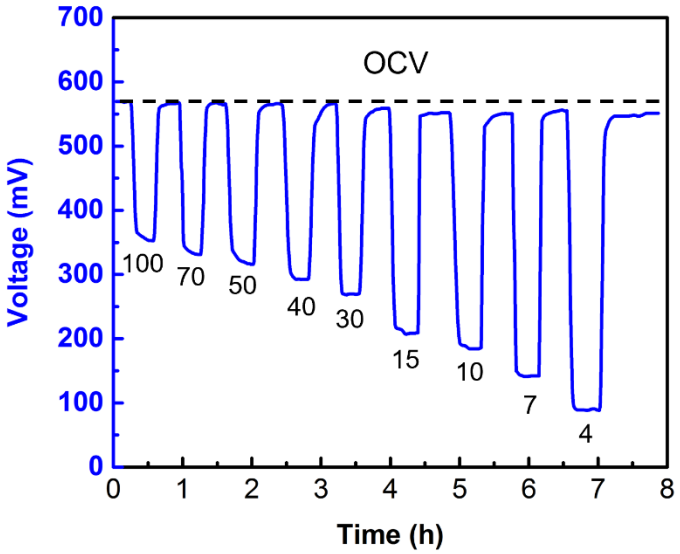

Fig. S7 Results from a typical polarization test obtained from a membrane MFC. Voltage was recorded versus time after switching between OCV and external resistances of to 100, 70, 50, 40, 30, 15, 10, 7, 4 kΩ. A total flow rate of Q_T=0.1 mL h^{-1}.

7. The volumetric flow rates and flow velocities

Important hydrodynamic properties such as contact time, diffusion distances and shear stress are related to the flow velocity. The relationship between flow velocity (v in units of m min^{-1}) and volumetric flow rate (Q_T in units of mL h^{-1}) is shown in the main paper in Equation 8. For the membrane device, the cross-section area was 0.35 mm^2, ignoring the volume occupied by the 50 µm-wide membrane in the membrane MFC. The cross-section area for membraneless MFC was 1.92 mm^2. To facilitate a better comparison between the two devices evaluated here we calculated the relationship between total volumetric flow rate and average velocity are given in Tables S1 and S2 for membraneless and membrane MFC devices, respectively.

Table S1 The volumetric flow rates and their responding flow velocities for membrane microfluidic MFCs with 0.8 mm electrode spacing.

Q_T (mL h^{-1})	ν (m min^{-1})	J_A (mol m^{-2} s^{-1})
0.1	4.7×10^{-3}	7.8×10^{-4}
0.2	9.5×10^{-3}	1.6×10^{-3}
0.5	2.4×10^{-2}	4.0×10^{-3}
1	4.8×10^{-2}	8.0×10^{-3}
3	1.4×10^{-1}	2.4×10^{-2}
5	2.4×10^{-1}	4.0×10^{-2}
10	4.8×10^{-1}	8.0×10^{-2}
20	9.6×10^{-1}	1.6×10^{-1}

Table S2 The volumetric flow rates and their responding flow velocities for membraneless microfluidic MFCs with 6 mm electrode spacing.

Q_T (mL h^{-1})	ν (m min^{-1})	J_A (mol m^{-2} s^{-1})
1	4.4×10^{-3}	7.3×10^{-4}
2	8.7×10^{-3}	1.4×10^{-3}
6	2.6×10^{-2}	4.3×10^{-3}
10	4.3×10^{-2}	7.6×10^{-3}
20	8.7×10^{-2}	1.4×10^{-2}
40	1.7×10^{-1}	2.9×10^{-2}
80	3.5×10^{-1}	5.8×10^{-2}
140	6.1×10^{-1}	1.0×10^{-1}

8. Profilometry and electrode profile

Characterization of the three-dimensional profile of the membrane MFC was conducted using an optical profilometer (ContourGT, Bruker Ltd., Canada). The measurements were conducted on an unbonded devices without liquid access holes punched. Fig.S8a shows the results with colour coding representing the height profile. Certain dimensions in the X-Y plane are also marked. From bottom to top the channel height was approximately 50 µm. The electrodes were integrated (dashed boxes in (a)) and their vertical profiles at the lower level were discernible thanks to the high resolution of the technique. The profile along the dashed white lines in (a) are plotted in Fig. S8b. Note the differences in units along the height (Z-axis) and downstream position (Y-axis) accentuates the protrusion of the electrode from the surface, but in reality each electrode protrudes between 6-12 µm). This was not a serious protrusion and the membrane formation proceeded well under such conditions. However, if greater protrusions (or recessions) was observed to have a negative impact effect on membrane formation.

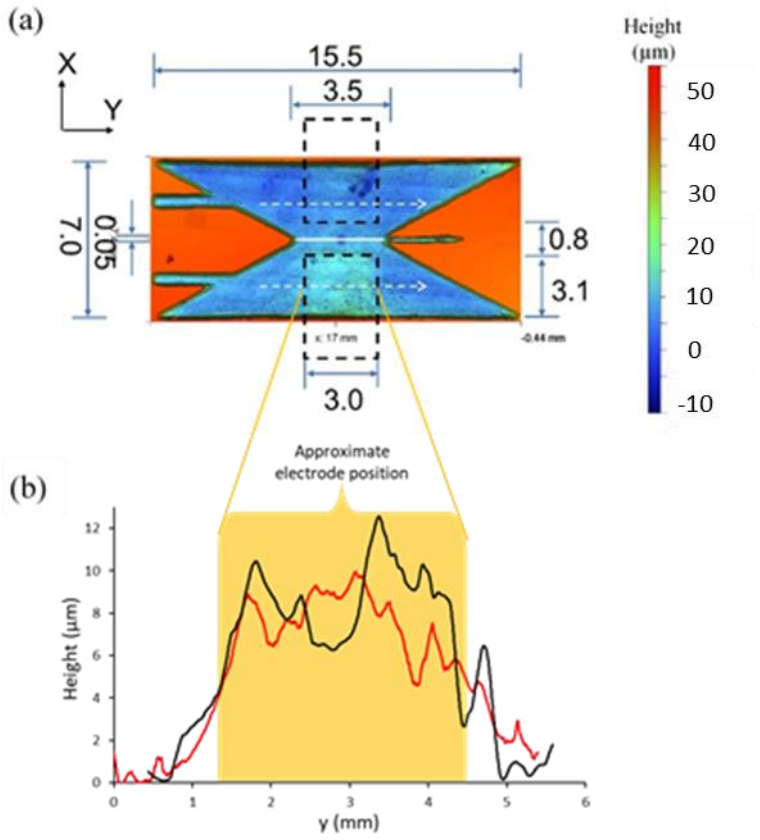

Fig. S8 (a) Isometric 3D schematic of a membrane microfluidic electrochemical flow cell showing two graphite electrodes (black), chitosan membrane (white part in the middle of the device), four inlets (Inlet 1 to 4 from top to bottom on the left) and three outlets (Outlet 1 to 3

from top to bottom on the right) and with dimensions indicated. (b) The height difference in Z-axis across an electrode indicated in white dotted arrow in (a). All units are in millimeters (mm).

9. Schematic of membrane and membraneless MFCs

Two microfluidic MFCs were used in this study. The membrane MFC was smaller (anode chamber, Vol_{anode}=1.4 µL) with electrodes that were in proximity (0.8 mm) as seen in Fig. S9a. For the membraneless MFC, the anode chamber volume was larger (V_{anode}=4.8 µL), featuring a relatively large electrode spacing (6 mm) as seen in Fig. S9b. The height of the membrane and membraneless devices were designed to be 150 and 160 µm, respectively.

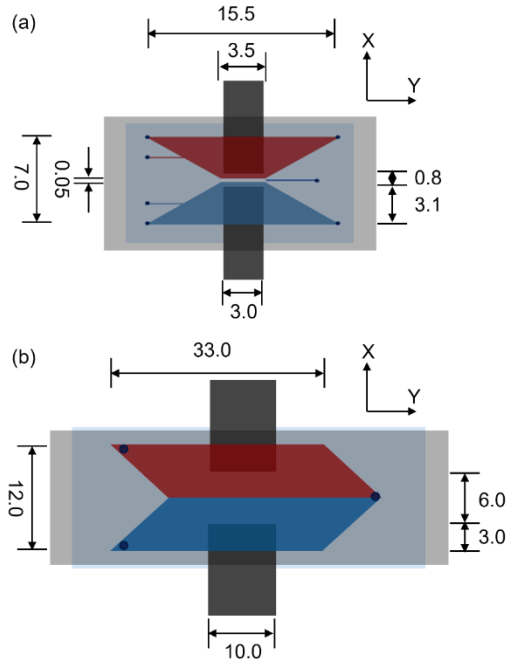

Fig. S9 Two-dimensional schematic of microfluidic MFCs bioelectrochemical flow cells with designs (a) for chitosan membrane and (b) membraneless design. Two graphite electrodes were shown in black with electrodes spacing for each figure. Anolyte and catholyte are indicated in red and blue domain in microfluidic MFCs respectively. All units are in millimeters (mm).

10. Convention on variable naming

We clarify the variable conventions used in this paper and how they relate to those in other fields, principally microfluidics and microbiology. It is standard for microfluidics users to refer to volumetric flow rates (volume per unit time) with the symbol Q, which we use here. We note that "f" is another symbol for volumetric flow rates that is often used by microbiologists.

In typical biofilm flow reactors, biofilms attached throughout the internal surface contribute to the reaction and the entire device constitutes the reaction chamber. In such an example, it can be useful to consider the hydraulic retention of the entire device, which is given by the total flow system volume divided by the volumetric flow rate (Eqn. S6). Its inverse gives the device dilution rate, $D=t_h^{-1}$ (s^{-1}) (Eqn. S7):

$$t_h\ (s)=Vol/Q_T \qquad \text{(Eqn. S6)}$$

$$D\ (s^{-1})=t_h^{-1} \qquad \text{(Eqn. S7)}$$

The context for t_h and D should be reconsidered in the case where the reaction occurs in a subsection of the flow system, such as the anode compartment in a microfluidic MFC. For example, dividing the anode chamber volume will return the same t_h for any anode chamber under the same flow rate as long as the cross-section area (and anode chamber volume) are the same. Whereas t_h, will clearly be longer if the same anode chamber were elongated along the direction of flow. In that example, Eqn. 1a captures the fact that t_h in the anode chamber increases, whereas Eqn. 11a does not.

Next, we consider (nutrient) supply rate, which is a controlling factor in cell growth rate in nutrient-limited conditions for typical bioflow cells. Again, considering the entire device as the growth chamber, the device supply rate (flow rate (Q) by the nutrient concentration) can be a relevant value. In the present case where the entire flow field does not contact the EAB because the anode chamber only occupies a fraction of one wall of the flow system, there is an oversupply of nutrients to the channel which does not contribute to growth due to bypass of the EAB. Even in the case of ubiquitous biofilm colonization of entire internal surface, one can appreciate that two devices with different surface area to volume ratios will access the supplied nutrients to a different degree. This difference may be minimal in macroscale flow cells, but the effect is amplified in microflow systems where surface area to volume ratios are extremely sensitive to changes in channel dimensions. For these reasons, we reformulate the concept of supply rate for the present microfluidic MFC by reducing the dimensionality of the flow to consider only the (linear) flow velocity, v ($m\ s^{-1}$). As shown in Eqn. 2 in the main paper, multiplying flow velocity by acetate concentration provides the convective flux. In the present work, the inlet acetate concentration is held constant at [Ac]=10 mM, so the flow velocity is always proportional to the convective nutrient flux. Finally, regulating nutrient flux is useful approach to normalizing the operational conditions of (and therefore to compare results)

between different MFCs. Therefore, in this work we ensure that the flow velocities are matched when comparing (larger volume) membraneless MFC and (smaller volume) membrane MFCs.

11. Supporting References

1. B. Averill, P. Eldredge, Principles of general chemistry, 1.0 ed. *Creative Commons,* **2012**.
2. H. N. Po, N.M. Senozan, *J Chem Educ*, 2001, **78**, 1499-1503.